

Low-cost phase change material as an energy storage medium in building envelopes: Experimental and numerical analyses [☆]



Kaushik Biswas ^{a,*}, Ramin Abhari ^b

^a Oak Ridge National Laboratory, One Bethel Valley Road, Oak Ridge, TN 37831, USA

^b REG Synthetic Fuels, LLC, Renewable Energy Group Inc., 5416 S. Yale, Tulsa, OK 74135, USA

ARTICLE INFO

Article history:

Received 23 July 2014

Accepted 1 September 2014

Keywords:

Phase change materials
Low-cost PCM
PCM modeling
Finite element analysis
COMSOL

ABSTRACT

A promising approach to increasing the energy efficiency of buildings is the implementation of a phase change material (PCM) in the building envelope. Numerous studies over the last two decades have reported the energy saving potential of PCMs in building envelopes, but their wide application has been inhibited, in part, by their high cost. This article describes a novel PCM made of naturally occurring fatty acids/glycerides trapped into high density polyethylene (HDPE) pellets and its performance in a building envelope application. The PCM–HDPE pellets were mixed with cellulose insulation and then added to an exterior wall of a test building in a hot and humid climate, and tested over a period of several months. To demonstrate the efficacy of the PCM-enhanced cellulose insulation in reducing the building envelope heat gains and losses, a side-by-side comparison was performed with another wall section filled with cellulose-only insulation. Further, numerical modeling of the test wall was performed to determine the actual impact of the PCM–HDPE pellets on wall-generated heating and cooling loads and the associated electricity consumption. The model was first validated using experimental data and then used for annual simulations using typical meteorological year (TMY3) weather data. This article presents the experimental data and numerical analyses showing the energy-saving potential of the new PCM.

© 2014 Elsevier Ltd. All rights reserved.

1. Introduction

According to the 2009 residential energy consumption survey (RECS)¹ of the United States Energy Information Administration (EIA), about 48% of the total residential end-use energy consumption is due to space heating and air conditioning. The U.S. Department of Energy (DOE) has set a goal of developing high-performance, energy-efficient buildings, which will require more cost-effective and energy-efficient building envelopes. Phase change materials (PCMs) have been widely investigated for thermal storage in a range of applications, including integrated collector storage solar water heat-

ing [1], spacecraft thermal control in extreme environments [2], phase change slurries for active cooling [3], thermal management of building integrated photovoltaic panels [4], etc. Application of PCMs to building envelopes to take advantage of their latent heat capacities in reducing the envelope-generated heating and cooling loads has received a lot of attention in the last two decades [5].

PCMs in building envelopes operate by changing phase from solid to liquid while absorbing heat from the outside and thus reducing the heat flow into the building, and releasing the absorbed heat when it gets cold outside to reduce the heat loss through the building envelope. Different approaches to PCM applications in building envelopes have been investigated: PCM wallboards [6,7], PCM mixed in concrete and brick [8,9], PCM mixed with loose-fill insulation [10,11], rigid polyurethane foam incorporating fatty acid ester based PCM [12], and macro-packaged PCM in plastic pouches [13,14]. Recent experimental and numerical studies have shown the potential of PCMs in reducing indoor temperature fluctuations under different weather conditions [15–17], reducing energy consumption and providing peak-load shifting [18], and also providing internal humidity control [16].

The energy saving potential of PCMs for buildings has been demonstrated, but the traditionally high PCM prices have precluded their extensive application in the building industry. This

[☆] Notice: This manuscript has been authored by UT-Battelle, LLC, under Contract No. DE-AC05-00OR22725 with the U.S. Department of Energy. The United States Government retains and the publisher, by accepting the article for publication, acknowledges that the United States Government retains a non-exclusive, paid-up, irrevocable, world-wide license to publish or reproduce the published form of this manuscript, or allow others to do so, for United States Government purposes.

* Corresponding author at: One Bethel Valley Road, Building 3147, P.O. Box 2008, M.S. – 6070, Oak Ridge, TN 37831, USA. Tel.: +1 (865) 574 0917; fax: +1 (865) 574 9354.

E-mail address: biswask@ornl.gov (K. Biswas).

¹ <http://www.eia.gov/consumption/residential/data/2009/index.cfm?view=consumption>.

Nomenclature

c_p	specific heat (kJ/kg/K)
F	view factor
$h(T)$	enthalpy (kJ/kg)
h_{ext}	exterior surface convective heat transfer coefficient (W/m ² /K)
h_{int}	interior surface heat transfer coefficient (W/m ² /K)
k	thermal conductivity (W/m/K)
L_f	latent heat of melting/freezing (kJ/kg)
q	heat flux (W/m ²)
q_{solar}	solar irradiance (W/m ²)
T	temperature (K)
α	solar absorptance
ε	infrared emittance
ρ	density (kg/m ³)

Subscripts

ext	exterior
int	interior
l	fully molten state of PCM
s	fully frozen state of PCM

Abbreviations

LWR	long wave radiation
NET	natural exposure test
OSB	oriented strand board
PCM	phase change material
RH	relative humidity

article is related to the evaluation of thermal performance of a new low-cost bio-PCM, with the end goal being the commercialization of the low-cost PCM. The production process of the bio-PCM involves two components: (1) on-purpose production of C₁₆–C₁₈ paraffins from low cost bio-renewable feedstock, and (2) low-cost encapsulation using under-water pelletizers. Bio-renewable feedstock such as low-value fats and greases, which do not compete with food crops, have been shown to be both sustainable and profitable feeds for production of biofuels – ester “biodiesel” and paraffinic “renewable diesel” [19,20], whose cost is similar to petroleum diesel. This new bio-based PCM is the intermediate product in the renewable diesel production process. Furthermore, the current petrochemical PCM paraffins (hexadecane and octadecane) command significantly higher prices than diesel fuels (bio-based and petroleum). Given the petrochemical PCM-vs-diesel price differential, the new bio-based paraffinic PCMs are indeed a sustainable, low-cost alternative to current PCMs.

Hexadecane (C₁₆H₃₄), heptadecane (C₁₇H₃₆), and octadecane (C₁₈H₃₈) are three paraffins that melt/freeze between 20 °C (64 °F) and 28 °C (82 °F), and have latent heats ranging between 152 and 244 kJ/kg [21]. The temperature range of 20–28 °C is considered the comfort zone for most people. High latent heat and a suitable phase change temperature range make these paraffins attractive as PCMs for building applications. Animal fats and vegetable oils contain 97% or higher C₁₆ and C₁₈ fatty acids, and can be converted to C₁₆–C₁₈ paraffins using a reaction called hydrodeoxygenation. Further, studies have shown that paraffins can be trapped into high density polyethylene (HDPE) by co-crystallizing a paraffin/HDPE melt. Up to 70% paraffin can be trapped in the HDPE matrix such that molten paraffin does not seep out of the solid HDPE matrix. Under-water pelletizers have been successfully used to convert molten polymer systems to pellets of various sizes, including <1 mm pellets. The combination of C₁₆–C₁₈ paraffin production from low-cost fats and waste vegetable oils, combined with a low-cost encapsulation method, is expected to result in a significant reduction in PCM production costs. Kosny et al. [22] performed an economic analysis to evaluate the cost effectiveness of PCM-enhanced building envelopes and determined the target cost levels at which PCMs can be cost competitive with conventional building thermal insulation materials. For a payback period of 10 years, assuming 30%-by-weight dispersed PCM in wall insulation, Kosny et al. [22] estimated cost targets of \$3.30–8.80/kg (\$1.50–4.00/lb) for PCMs with latent heats varying between 120 and 220 kJ/kg. The cost of the current PCM with a latent heat of 116 kJ/kg [23] is projected to be about \$4.40–6.60/kg (\$2–3/lb) or less, when manufactured at a commercial scale.

As mentioned earlier, there are several studies evaluating building applications of PCMs [5–18]. Al-Saadi and Zhai [24] reviewed the modeling of PCMs in building enclosures and highlighted the issues needing further research, with one of the research needs being quantification of PCM modeling performance under different climatic and operating conditions [24]. Recently, Biswas et al. reported a combined experimental and numerical evaluation of a nano-PCM containing gypsum board [25]. The PCM–gypsum board was tested in a natural exposure test (NET) facility in a hot and humid climate over a period of several months. Finite-element models of the test wall were built and validated against the test data (temperature and heat flows), and then used to evaluate the energy-saving potential of the PCM–gypsum board through annual simulations [25].

This article describes another test wall, tested at the same NET facility, containing the new low-cost bio-PCM. The PCM-containing HDPE pellets were dispersed in cellulose insulation for filling in wall cavities. The primary difference between the previous nano-PCM study [25] and the current study is the manner of incorporating PCMs in the building envelope. Similar to the nano-PCM study, two-dimensional finite element models of wall assemblies were created and validated against data from the NET building, and then used for annual simulations of the PCM–HDPE pellets mixed with cellulose insulation (or ‘PCM–cellulose insulation’ in further discussions). In the following sections, the test wall is briefly described, followed by descriptions of the experimental testing and numerical modeling methodology, and finally, the performance of the PCM–cellulose insulation is compared to regular cellulose insulation. The test facility and the simulation methodology are the same as described by Biswas et al. [25], but for convenience, the details have been repeated in this article.

2. Test facility and test wall details

The NET facility is located in Charleston, South Carolina and is used for testing building envelope assemblies by exposing them to natural weathering. Fig. 1 shows the southeast wall of the Charleston NET facility, which houses multiple side-by-side test walls. Also shown is a weather station on the southwest gable end of the building. Fig. 2 shows the test wall construction. The test wall was divided into four sections, indicated by A–D in Fig. 2. Section ‘A’ was filled with regular cellulose insulation and ‘B’ contained the PCM–cellulose insulation. The regular cellulose insulation section was used as a baseline. Two additional sections were created: section ‘C’ containing a mixture of cellulose and HDPE pellets without the paraffin, and section ‘D’ containing a sandwiched

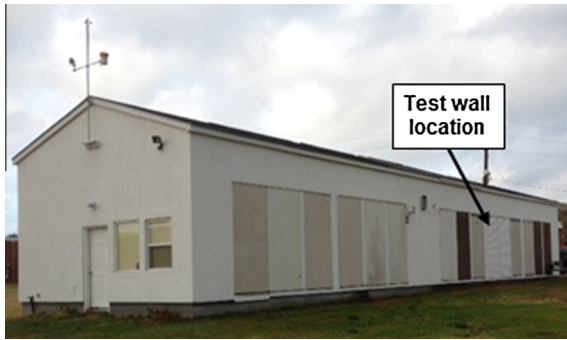


Fig. 1. Charleston, SC natural exposure test (NET) facility.

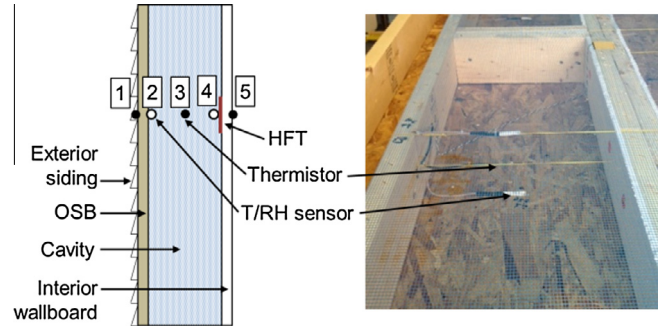


Fig. 3. Sensor placement in test wall.

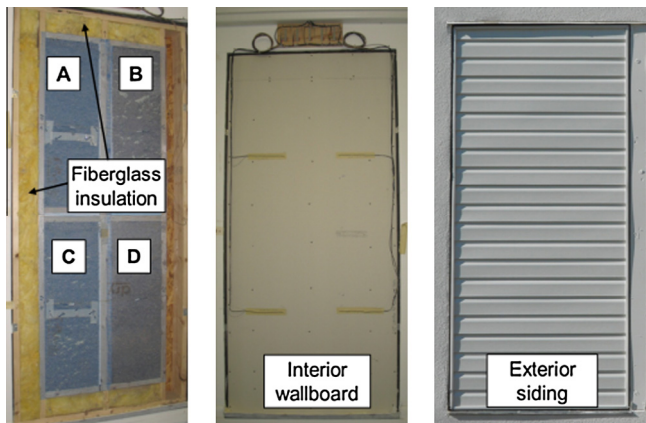


Fig. 2. Left: Test wall construction – (A) regular cellulose insulation, (B) PCM–cellulose insulation, (C) cellulose–HDPE mix, and (D) cellulose–PCM–cellulose sandwich structure. Center: finished interior. Right: finished exterior with vinyl siding.

configuration of a PCM–HDPE layer between layers of cellulose. However, sections ‘C’ and ‘D’ are not the focus of this article since they were created purely for testing purposes and their configurations did not represent how the PCM is intended to be installed in actual buildings. In this article, further details, experimental data and simulations results of sections ‘A’ and ‘B’ only are presented since ‘B’ is the preferred mode of installation for the PCM and ‘A’ is the baseline condition.

The wall was built using 2×6 wood studs, resulting in a wall cavity depth of 14 cm (5.5 in.), with a 1.3 cm (0.5 in.) oriented strand board (OSB) attached to the exterior side of the wall. The cavity dimensions were $1.1 \times 0.4 \text{ m}^2$ (42.4×14.5 square inch). The nominal amount of PCM in the PCM–cellulose insulation was 20% by weight. The PCM–HDPE pellet design was such that the pellets contained 66% paraffin by weight. Thus, the PCM–HDPE pellets and cellulose were mixed so that the mixture contained 30%-by-weight pellets, or 0.45 kg of pellets for each kg of cellulose. The in-situ density of the PCM–cellulose mixture was 61.6 kg/m^3 (3.85 lb/ft^3). The in-situ density of the cellulose insulation was 40.8 kg/m^3 . It should be noted that the cellulose insulation (regular and mixed with the PCM–HDPE pellets) was filled in the cavities from the top and allowed to settle under its own weight. Therefore, the densities of the cellulose and PCM–cellulose insulation were expected to be different from typical residential wall applications of blown-in cellulose.

Once installed, the outer cavities of the test wall were filled with fiberglass insulation to thermally insulate the wall from the other neighboring test walls, as shown in Fig. 2. Further, any gaps observed at the top of the cavities (due to settling of the cellulose

Table 1
Installed sensor accuracy.

Sensor	Accuracy (%)	Sensitivity	Repeatability (%)
10 K ohm thermistor	± 0.2	–	± 0.2
Humidity sensor	± 3.5	–	± 0.5
Heat flux transducer	± 5	$(5.7 \text{ W/m}^2)/\text{mV}$	–

insulation) were filled with more cellulose insulation. Fig. 2 also shows the finished interior and exterior faces of the test wall. The interior side was covered with 1.3 cm (0.5 in.) gypsum board and the exterior OSB was covered with a weather resistive barrier (0.15 mm thick high density polyethylene sheet) followed by vinyl siding. Also visible on the interior face are four (4) temperature sensors, one centered on each section/wall cavity.

2.1. Data acquisition system and instrumentation

Fig. 3 shows a typical instrumentation layout in the wall sections. Each section contained a thermistor and relative humidity (RH) sensor combination (T/RH sensor) on the OSB and gypsum surfaces facing the cavity, a thermistor inside the cavity (mid-depth) and on the gypsum surface facing the room interior, and heat flux transducers on the gypsum surface facing the cavity. Within each section, these sensors were located approximately in a line along both the vertical and horizontal midpoints of the section. In addition, a single thermistor was attached to the wall exterior (interior face of the siding) and a T/RH sensor combination was attached on the OSB surface facing the exterior (not shown in Fig. 3).

The NET facility also contained sensors and instruments to monitor the local weather conditions, including temperature, humidity, solar irradiance and wind velocity. Each sensor was scanned at five minute intervals and the data were averaged and stored at hourly intervals. The data were downloaded on a weekly basis using a dedicated computer and modem. Table 1 provides the sensor specifications.

3. Numerical simulations

To evaluate the impact of the PCM–cellulose insulation on wall-generated heating and cooling loads, numerical modeling was required. Since both the test wall sections (with PCM–cellulose and cellulose-only insulation) were interacting with the same interior conditioned space, it was difficult to isolate their individual energy benefits. Therefore, two-dimensional (2D) finite element models were created using COMSOL Multiphysics (version 4.3a)² to analyze the PCM performance.

² <http://www.comsol.com/>.

Table 2
Material properties for numerical modeling.

	Density (kg/m ³)	Thermal conductivity (W/m/K)	Specific heat (kJ/kg/K)	Latent heat (kJ/kg)
Cellulose	40.8	0.042	1.424	–
Wood stud	576.7	0.144	1.633	–
OSB	640.0	0.130	1.410	–
Foam (expanded polystyrene)	24.0	0.037	1.214	–
Gypsum	549.5	0.153	1.089	–
PCM–HDPE pellets	505.3	–	–	116.7
PCM–cellulose insulation	61.7	0.051(s) 0.046 (l)	– –	– –

3.1. Methodology

In this section, a brief description of the numerical analysis methodology is provided. The first task was to check if the numerical models were capturing the thermal behavior of the actual test wall. For this purpose, 2D wall models were created, with identical dimensions as the test wall and using thermo-physical properties of the materials used in the test wall. The model calculation results were then compared to the experimentally measured temperatures and heat flows, for validation.

Following model validation, annual simulations were performed to estimate the energy benefits of the PCM–cellulose insulation. Following list provides a synopsis of the annual simulation work:

1. Appropriate exterior and interior boundary conditions were required for the annual simulation models. For the exterior side, data from typical meteorological year (TMY3)³ weather files were used. On the interior side, an assumed constant surface heat transfer coefficient was used to calculate the heat transfer between the wall surface and the interior conditioned space (room).
2. Heat gains and losses at the interior wall surface were calculated and used for comparing the performance of PCM–cellulose and cellulose-only insulation.
3. In the simulations, the room temperature was allowed to float between, but was limited to, the assumed heating and cooling temperature set points.
4. The impact of the location of the PCM in walls was evaluated using four scenarios: (i) no PCM, (ii) PCM dispersed throughout the wall cavity, (iii) PCM dispersed in the inner half (towards the room), and (iv) PCM dispersed in the outer half (towards the exterior).
5. Finally, the impact of PCM–cellulose insulation on wall-generated heating and cooling electricity consumption was investigated. This was done by converting the calculated wall heat gains and losses to electricity consumption, using typical temperature-dependent coefficients of performance (COP) of heat pumps.

All the above are described in detail in the next subsections and ‘Section 4’.

3.2. Material properties

Table 2 lists the material properties used for numerical modeling. These values were obtained from literature or through measurements.

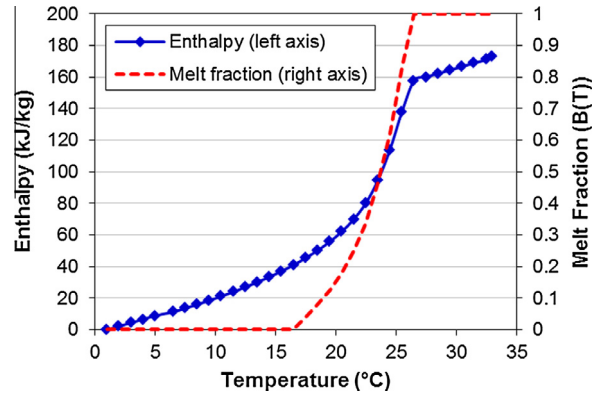


Fig. 4. Enthalpy of PCM–HDPE pellets as a function of temperature [23].

The cellulose and PCM–cellulose densities were the same as the in-situ densities in the actual test wall. The specific heat and latent heat of the PCM–HDPE pellets were obtained from differential scanning calorimetry (DSC) tests, reported by Shukla et al. [23]. Fig. 4 shows the enthalpy (h) of the PCM–HDPE pellets as a function of temperature, based on the DSC data. The specific heat (c_p) of the pellets was calculated as,

$$c_{p,HDPE}(T) = \frac{dh(T)}{dT} \quad (1)$$

Since the weight ratio of the pellets and cellulose in the PCM–cellulose insulation was 30:70, the specific heat of the PCM–cellulose insulation was,

$$c_{p,PCM-cellulose}(T) = 0.3 \cdot c_{p,HDPE}(T) + 0.7 \cdot c_{p,cellulose}(T) \quad (2)$$

The enthalpies were calculated using the average of the heat gain/loss data from the melting and freezing DSC tests. In general, the phase change enthalpy is not an identical function of temperature during melting and freezing of PCMs. This phenomenon in PCMs is referred to as ‘hysteresis’ and it is particularly significant with certain types of PCM, for example inorganic PCMs. However, past research has shown that, at slow heating and cooling rates, the hysteresis effect in paraffinic PCMs, such as the present PCM–HDPE pellets, is negligible [26]. The measured rate of diurnal temperature fluctuations of the current test wall was limited to less than 1 °C/h. Thus, using an averaged enthalpy as a function of temperature was deemed a reasonable approximation for the current simulations.

The phase change or melting onset and end temperatures of 16.5 °C and 26.5 °C, respectively, were calculated from the measured PCM enthalpy ($h(T)$) using the procedure described in ASTM C1784 [27]. The latent heat (L_f) of 116.7 kJ/kg was calculated as the difference in enthalpy between the phase change onset and end temperatures. Fig. 4 also shows the melt fraction ($B(T)$) of the PCM as a function of temperature. The melt fraction was calculated as,

$$B(T) = \begin{cases} 0, & h < h_s \\ (h - h_s)/L_f, & h_s \leq h \leq h_l \\ 1, & h > h_l \end{cases} \quad (3)$$

In the above equation, h_s is the enthalpy at the melting onset temperature and h_l is the enthalpy at the melting end temperature. The subscripts, ‘s’ and ‘l’, indicate solid and liquid states, respectively.

The thermal conductivity of PCM–cellulose insulation was defined as,

$$k(T) = k_s + (k_l - k_s)B(T) \quad (4)$$

³ http://rredc.nrel.gov/solar/old_data/nsrdb/1991-2005/tmy3/.

' k_s ' and ' k_l ' are the thermal conductivities of the PCM–cellulose when the PCM was fully frozen and fully molten, respectively. They were measured according to ASTM C518 [28] and are listed in Table 2.

3.3. Model validation

The finite element numerical models had to be validated against experimental data to ensure that they could capture the thermal behavior of the test wall components. Two-dimensional (2D) models of the actual test walls were created. Fig. 5 shows the model geometry, which replicates a horizontal 2D cross-section of the test wall. The section shows a plan view corresponding to the horizontal centerline of the upper test wall sections (shown in Fig. 2). The 2D wall section was divided into two cavities, divided by wood studs and foam insulation in the middle, with regular cellulose and PCM–cellulose insulation in the two cavities, same as the test wall. The wall model geometry contained gypsum board on the interior side and OSB on the exterior side. The model wall geometry was created according to the actual dimensions of the test wall.

Fig. 5 also shows the locations of 'thermistors' and 'HFTs' in the model geometry. These were locations within the model geometry where the simulation results were monitored and used for comparison with the experimental data. These locations were chosen to be as close as possible to the actual sensor locations in the test wall (Fig. 3). The 'thermistor' near the wallboard surface facing the cavity was offset. This is because the T/RH sensors in the actual test wall were not attached to the exterior face of the internal wallboards, but were slightly pushed inside the cavities once they were filled with insulation.

The model solved the following time-dependent energy equation,

$$\rho \frac{\partial h}{\partial t} = \nabla \cdot (k \nabla T), \text{ where } h = \int c_p dT \quad (5)$$

In Eq. (6), ' ρ ' is the density, ' h ' is the enthalpy, ' k ' is the thermal conductivity and ' c_p ' is the specific heat of the different wall materials. Exterior and interior wall surface temperatures from the experimental data were used as boundary conditions on the exterior and interior surfaces, respectively. Insulated, or adiabatic, boundary conditions were assumed at lateral edges of the wall model (top and bottom edges of the test wall section in Fig. 5), which is appropriate since the area surrounding the test wall sections/cavities was filled with fiberglass insulation (Fig. 2).

3.4. Annual simulations using TMY3 data

Once the 2D finite element models were validated against experimental data, they were used for annual simulations. Fig. 6

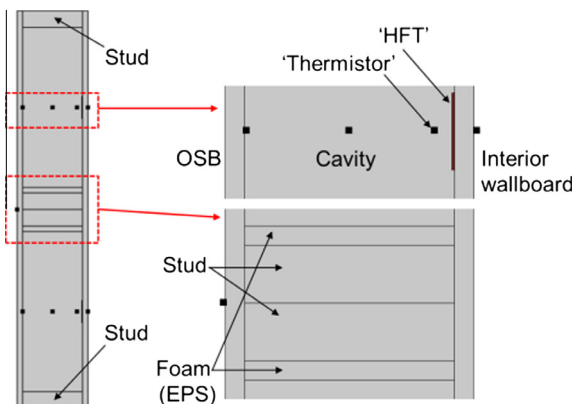


Fig. 5. Model geometry representing a horizontal cross-section of the Charleston test wall, used for validation of the numerical model.

shows the simplified wall geometry that was used for the annual simulations. The wall construction used in the model was '2 × 6' stud construction, i.e. it contained wood studs of 3.8 cm × 14.0 cm (1.5 in. × 5.5 in.), resulting in a cavity depth of 14.0 cm (5.5 in.). The centerline of the studs were spaced 61 cm apart (24 in. on center). The exterior side consisted of 1.3 cm OSB and the interior contained 1.3 cm gypsum board. Simulations were performed with cellulose insulation and PCM–cellulose insulation in the wall cavity, to evaluate the energy-saving potential of the PCM.

The scope of the study was limited to calculating heat flows through a 'clear' section of the wall, i.e. no features other than the wall cavity and stud were modeled. No wall-wall or wall-ceiling interfaces, joints and corners, windows, etc., were considered in the model. Further, internal loads, solar gain and heat flow through windows, roof and ceiling loads, infiltration, etc. were not considered. Hence, only a small two-dimensional (2D) horizontal cross-section of the wall was modeled, extending from the stud centerline to the cavity centerline. Exterior boundary conditions were applied to the OSB surface that is exposed to the "outside" and an interior boundary condition was applied to the interior wallboard surface facing the "room". Symmetry boundary conditions were assumed at the stud and cavity centerlines, as indicate in Fig. 6.

Appropriate exterior and interior boundary conditions were required for the annual simulations. The exterior boundary conditions were estimated using typical meteorological year (TMY3) weather data for Charleston. Input files containing hourly values of outdoor and sky temperatures, solar radiation and exterior surface convective heat transfer coefficients were generated for the annual simulation models. Simulations were performed for walls oriented in all four directions: east, west, north and south.

The following external (q_{ext}) and internal (q_{int}) heat flux boundary conditions were imposed on each wall:

$$q_{ext} = \alpha q_{solar} + h_{ext}(T_{out} - T_{surf}) + \varepsilon \sigma [(1 - F_{sky})(T_{out}^4 - T_{surf}^4) + F_{sky}(T_{sky}^4 - T_{surf}^4)] \quad (6)$$

$$q_{int} = h_{int}(T_{room} - T_{surf}) \quad (7)$$

In the above equations,

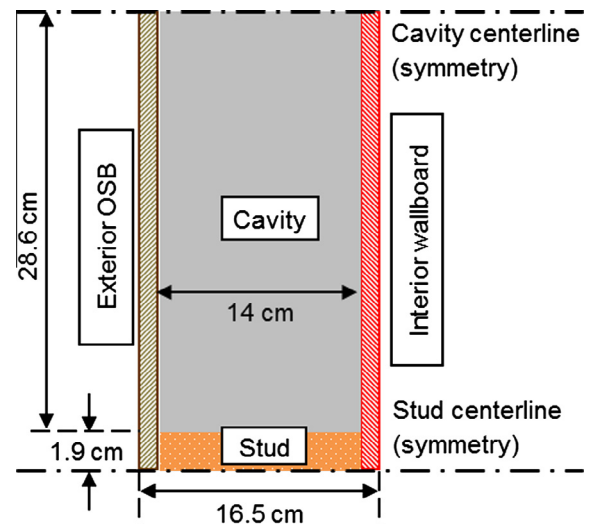


Fig. 6. Simplified model geometry for annual simulations.

- α = Solar absorptance of the exterior wall surface, assumed to be 0.6.
- ε = Infrared emittance of the exterior wall surface, assumed to be 0.8.
- q_{solar} = Solar irradiance on the exterior wall surface (W/m^2), from TMY3 data.
- h_{ext} = Exterior surface convective heat transfer coefficient ($W/m^2/K$).
- h_{int} = Interior surface heat transfer coefficient ($W/m^2/K$).
- F_{sky} = Radiation view factor from sky to the wall.
- T_{out} = Outside ambient temperature (K), from TMY3 data.
- T_{sky} = Sky temperature (K), from TMY3 data.
- T_{surf} = Wall surface temperature (K); exterior wall surface facing the outdoor environment in Eq. (6) and interior surface facing the room in Eq. (7).
- T_{room} = Room (interior conditioned space) temperature (K).

In Eq. (6), the first term on the right side is the solar irradiance, the second term is the convection heat transfer and the last term is the long-wave radiation (LWR) exchange with the surroundings.

The exterior convective heat transfer coefficient (h_{ext}) was not a constant. Hourly values of ' h_{ext} ' were calculated using the outdoor temperature and wind velocity data from the TMY3 files. Hourly values of ' q_{solar} ' and ' h_{ext} ' for the different wall orientations were generated with the help of EnergyPlus⁴, a whole-building modeling tool.

The LWR heat transfer consists of radiation exchange between the exterior wall surface and the outside environment ('out'), ground and sky, and is given by:

$$q_{LWR} = \varepsilon\sigma[F_{out}(T_{out}^4 - T_{surf}^4) + F_{ground}(T_{ground}^4 - T_{surf}^4) + F_{sky}(T_{sky}^4 - T_{surf}^4)] \quad (8)$$

The outside air temperatures (T_{out}) were obtained from TMY3 data. F_{sky} , F_{out} and F_{ground} are the view factors between the exterior wall surface and the sky, outside and ground, respectively. For simplicity, the ground temperature (T_{ground}) was assumed to be the same as the outside air temperature (T_{out}), reducing the above equation to:

$$q_{LWR} = \varepsilon\sigma[(F_{out} + F_{ground})(T_{out}^4 - T_{surf}^4) + F_{sky}(T_{sky}^4 - T_{surf}^4)] \quad (9)$$

The sum of the three view factors (F_{sky} , F_{out} and F_{ground}) for a vertical exterior wall surface is unity.

$$F_{sky} + F_{out} + F_{ground} = 1 \quad (10)$$

Following Walton [29], the view factors were calculated as:

$$F_{sky} = \beta[0.5(1 + \cos \phi)]; \beta = \sqrt{0.5(1 + \cos \phi)} \quad (11)$$

where ϕ is the tilt angle of the surface from the horizontal, which is 90° for the walls being modeled. The following common assumptions were made for the radiation calculations:

- each surface emits or reflects diffusely and is gray and opaque,
- each surface is at a uniform temperature, and
- energy flux incident on or leaving a surface is evenly distributed across the surface.

The interior heat transfer coefficient (h_{int}) was assumed to be 8.29 $W/m^2/K$, following ASHRAE Handbook of Fundamentals⁵, for a non-reflective vertical surface. It was assumed that the heating and cooling systems could exactly match the instantaneous loads, so that the interior room temperature (T_{room}) floated between the heating and cooling set points but never went outside that range.

4. Results and discussion

In this section, the measured temperature and heat flux data, model validation as well as annual simulations and analyses are described. The section containing cellulose insulation mixed with HDPE-PCM pellets is referred to as 'PCM-Cellulose' and the section with only cellulose insulation is referred to as 'Cellulose' in the forthcoming discussions.

4.1. Sample temperature and heat flux data

Fig. 7 shows the measured temperature distribution in the 'PCM-Cellulose' and 'Cellulose' sections during three (3) summer days (July 12–15, 2012). Within each section, the measurement locations were exterior surface of the OSB ('OSB Ext. '), OSB surface facing the cavity ('OSB Int. '), the center of the cavity ('Cavity'), gypsum surface facing the cavity ('Gypsum Ext. ') and gypsum surface facing the room ('Gypsum Int. '). Fig. 8 shows the measured heat fluxes from the 'PCM-Cellulose' and 'Cellulose' sections, and the incident solar radiation on the exterior surface.

The room interior was maintained at about 20–22 °C during the monitoring period. The temperature distributions in both wall sections showed a clear trend from the exterior to the interior. Some differences were seen in temperatures at the cavity center and the wallboard exterior between 'PCM-Cellulose' and 'Cellulose' sections. However, the temperature differences were fairly insignificant and did not reveal much about the behavior and impact of the PCM. The heat gains, as measured by the HFTs, were discernibly lower through the 'PCM-Cellulose' section compared to the 'Cellulose' section. Similar trends were observed during the other seasons, depending on the outside conditions.

Two sources of uncertainties in the experimental measurements need to be noted. One was the potential for formation of air gaps in the cavities due to settling of cellulose insulation under its own weight. Fig. 9 shows the cavity insulation with the gypsum wallboard removed. The left image shows some air gaps near the sensor locations. Further, the PCM pellets and cellulose mixing and installation method was such that it was difficult to obtain a uniform distribution of the PCM pellets within the cellulose insulation. Fig. 9 also shows how the PCM pellets were concentrated in certain regions within the cavities. It was expected that the stratification of the PCM pellets will have an impact on the measured temperatures and heat fluxes, depending on the location of the sensors with respect to the concentration of the pellets. Some sample measurements were taken by installing two additional temperatures sensors at mid-cavity depth at two different heights within the 'PCM-Cellulose' section. The measured mid-cavity temperatures varied by up to 5 °C (9 °F), depending on the vertical location and concentration of pellets. Such variability in distribution could also impact the measured heat flows through the sections containing PCM pellets. A potential future task is to determine an installation method that can provide a more uniform distribution of the PCM in the insulation.

Since both the 'PCM-Cellulose' and 'Cellulose' sections were interacting with the same interior space, it was difficult to isolate their energy impacts through purely experimental means. For further evaluation and estimation of energy savings due to the PCM-cellulose insulation, numerical modeling was utilized.

4.2. Model validation using measured data

In Figs. 10 and 11, the calculated temperatures from the finite element model are compared to the experimentally measured temperatures from the test wall during three summer and three winter days, respectively. '[C]' indicates the model calculations

⁴ http://apps1.eere.energy.gov/buildings/energyplus/energyplus_about.cfm.

⁵ <https://www.ashrae.org/resources-publications/handbook>.

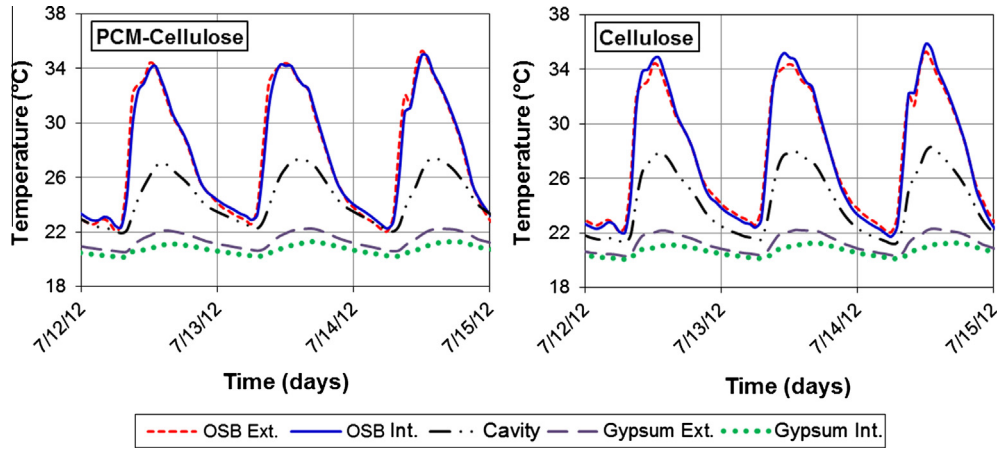


Fig. 7. Experimentally measured temperatures at different locations within the test wall during three summer days.

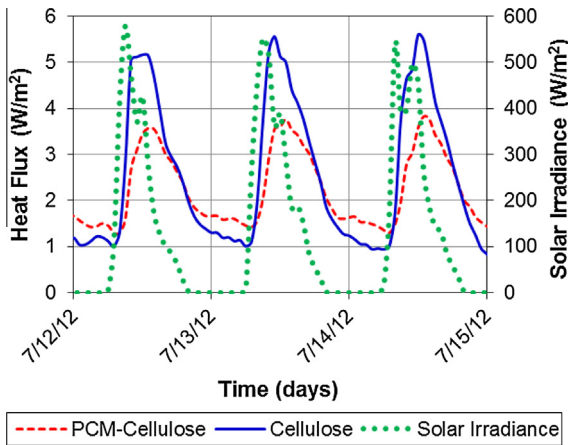


Fig. 8. Experimentally measured heat flows through the different test wall sections and solar irradiance on the wall exterior surface during three summer days.

using COMSOL. The monitored temperature locations were as shown in Figs. 3 and 5. Measured ‘OSB Ext.’ and ‘Gypsum Int.’ temperatures were used as the exterior and interior temperature boundary conditions, and temperature measurements from the other sensors were used for validating the model calculations. There was excellent agreement between model calculations and experimental data for almost all locations during summer and winter. The only location where some differences were observed

was the cavity center (‘Cavity’) in the ‘PCM–Cellulose’ section, under summer conditions. The differences can partly be explained by the PCM–cellulose composition. The model assumes uniform distribution of PCM within cellulose, which was not the case with the actual test wall cavity (Fig. 9). The non-uniform PCM distribution in the test wall was observed to have an impact on the temperature distribution with the ‘PCM–Cellulose’ section, as noted in the previous section.

Fig. 12 compares the calculated and measured heat fluxes through the ‘PCM–Cellulose’ and ‘Cellulose’ sections. HFTs were incorporated in the numerical model using the same dimensions and material properties as the HFTs installed in the actual test wall. Reasonable agreement between the calculations and measurements was observed for the winter period. However, the calculations based on summer conditions did not match very well with the measured data. While two sources of uncertainties in the measurements have been noted earlier, the exact reasons for such poor agreement between measurements and calculations of summer heat fluxes are unknown. Another potential reason could be the variable behavior of the PCM under different weather conditions and its impact on the test wall.

Overall, with their limitations noted, the numerical models were deemed adequate to capture the general behavior of the test wall sections and provide an estimate of the energy-saving potential of the PCM through annual simulations. If the current analyses show evidence of potential for substantial energy savings, future research will be viable for further improving the numerical model as well as more testing under improved experimental conditions.

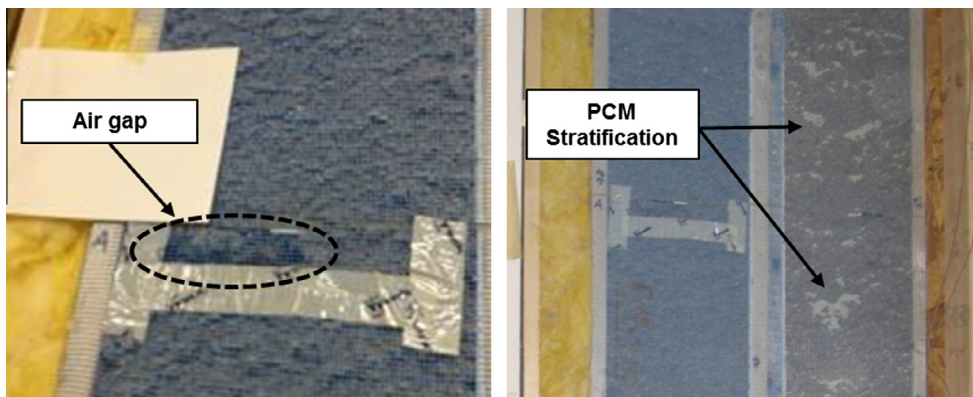


Fig. 9. Sources of uncertainties in experimental data: left – air gaps within the cavity insulation, right – stratification of PCM pellets within cellulose insulation.

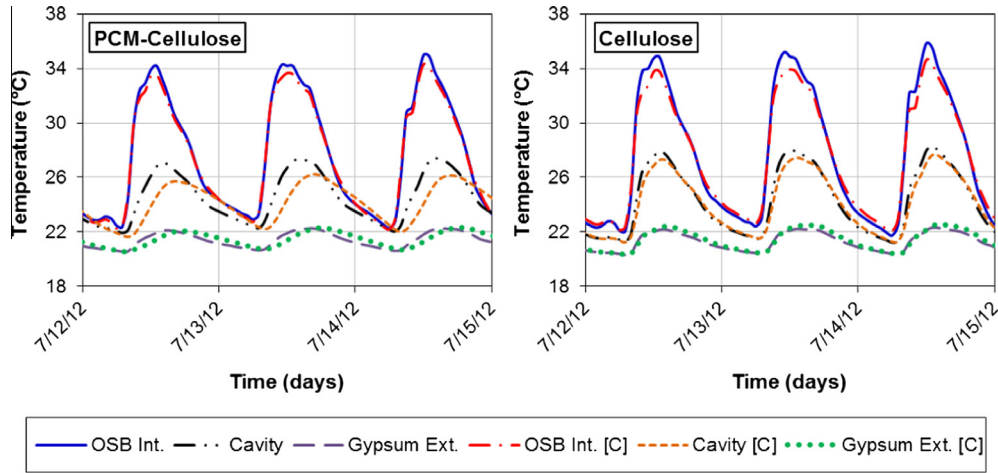


Fig. 10. Comparison of model calculations (indicated by [C]) with measured temperature data (summer).

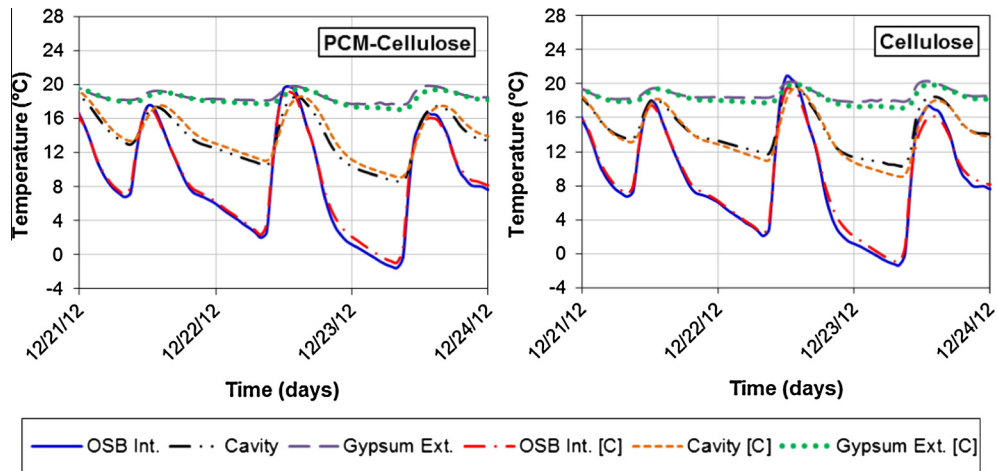


Fig. 11. Comparison of model calculations (indicated by [C]) with measured temperature data (winter).

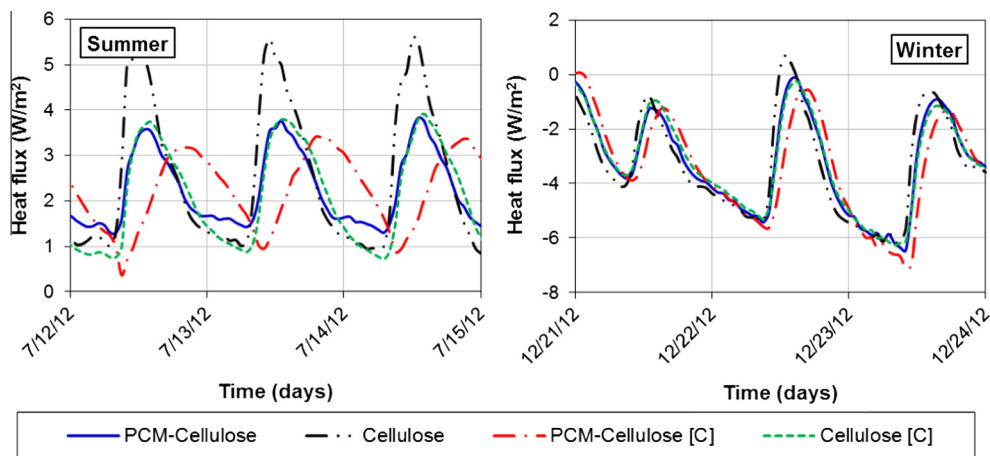


Fig. 12. Comparison of model calculations (indicated by [C]) with measured heat flux data.

4.3. Annual simulations

4.3.1. Calculated wall heat gains and losses

Table 3 lists the total annual heat gains and losses through the different modeled wall sections with ‘Cellulose’ and ‘PCM-

Cellulose’ insulation, using the exterior and interior boundary conditions described in Section 3.4. Heat gains and losses at the interior wall surface were calculated and used for comparing the performance of PCM-cellulose and cellulose-only insulation. The heating and cooling set points for the room were assumed to be

Table 3

Annual wall heat gains and losses at different orientations with 'Cellulose' and 'PCM–Cellulose' insulation, using 20–23.3 °C (68–74 °F) room temperature set points.

Wall orientation	Heat gain (Wh/m ²)		% Difference	Heat loss (Wh/m ²)		% Difference
	Cellulose	PCM–Cellulose		Cellulose	PCM–Cellulose	
East	10,451	10,307	–1.4	–7,820	–8,335	6.6
West	10,143	9,754	–3.8	–8,139	–8,582	5.4
North	5,761	5,769	0.1	–10,110	–11,339	12.2
South	11,289	10,088	–10.6	–6,524	–6,039	–7.4

20 °C (68 °F) and 23.3 °C (74 °F), respectively, which is fairly typical for buildings in the US. Different wall orientations receive different amounts of annual solar irradiance, which is reflected in the total heat gains through the walls. The annual heat losses through the different walls also varied substantially, with the highest heat loss associated with the north wall.

The calculated heat gains were observed to be higher than the heat losses through all walls, except the north wall, which is expected since Charleston lies in a hot and humid climate zone. The PCM–cellulose insulation reduced annual heat gains compared to cellulose-only insulation for all wall orientations, except the north wall. However, the total annual heat losses were higher with the PCM–cellulose insulation for all but the south-oriented wall. It should be noted that the walls in different orientations were modeled independently of one another. Therefore, the calculated heat gains and losses as well as any reductions in heat flows due to the PCM for each wall orientation was not impacted by the behavior of the other walls. This inter-wall independence is in addition to the fact the calculations did not consider any other architectural feature, as noted in Section 3.4.

4.3.2. Impact of PCM location and amount on the simulated results

Childs and Stovall [30] performed an optimization study of the impact of PCM incorporated in the cavity insulation in walls and investigated various parameters with respect to their effect on energy-savings resulting from the PCM. An important finding was that the calculated wall-related energy consumption was influenced by the location and concentration of PCM within the wall cavity [30]. Therefore, in the current study, annual simulations were performed with two additional model wall configurations. The wall cavity was assumed to be divided into two halves, one each towards the wall interior and exterior. The first additional configuration contained 'PCM–Cellulose' insulation in the inner half and cellulose-only insulation in the outer half; the other configuration was the opposite with 'PCM–Cellulose' outside and 'Cellulose' inside. The composition of the PCM–cellulose was the same in all scenarios, which means that in the models with the PCM–cellulose in outer or inner halves, the amount of PCM was half as compared to the full width PCM–cellulose configuration.

The south and north walls, with the highest heat gains and losses, respectively, have been discussed here for detailed evaluation. Fig. 13 shows the hourly heat gains through the south wall during three typical summer days, with hot and sunny conditions (based on the TMY3 data), for the different PCM configurations: 'No PCM' (cellulose-only insulation), 'Full width' (PCM–cellulose insulation in the full wall cavity), and 'Inner half' (PCM–cellulose in the inner half and cellulose-only in the outer half). Both the 'Full width' and 'Inner half' configuration reduced and delayed the peak heat gains through the south wall. During the night-time and early-morning hours, the heat gains with the 'Full width' and 'Inner half' configurations was higher than the 'No PCM' configuration, presumably due the exothermic freezing process of the PCM releasing its latent heat. If some means of removing this latent heat of freezing can be devised, so it is not released into the room, higher energy savings can be realized.

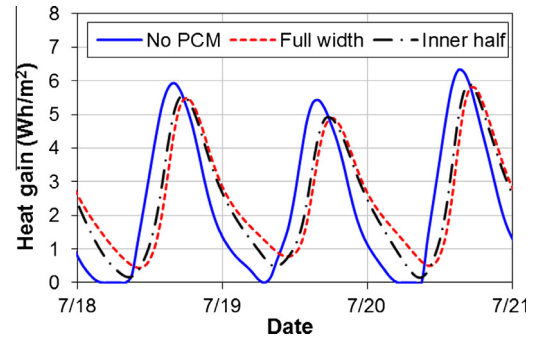


Fig. 13. Calculated heat gains through the south wall during three summer days, with different PCM configurations.

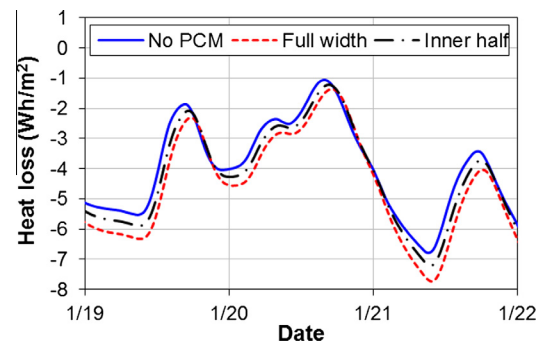


Fig. 14. Calculated heat losses through the north wall during three winter days, with different PCM configurations.

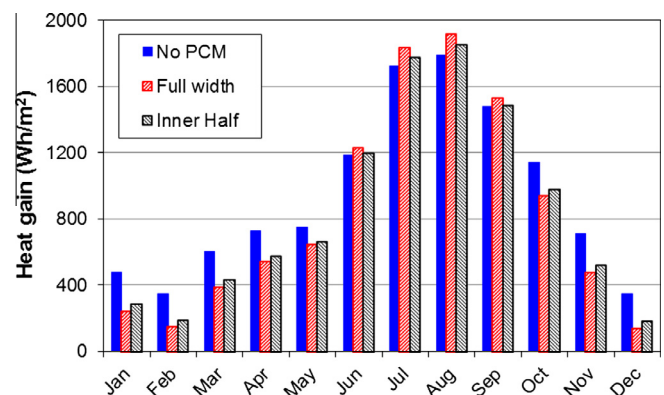


Fig. 15. Calculated monthly heat gains through the south wall, with different PCM configurations.

Fig. 14 shows the calculated hourly heat losses through the north wall during three winter days, also based on TMY3 data. The heat losses were highest for the 'Full width' configuration, followed by the 'Inner half' and 'No PCM' configurations. The

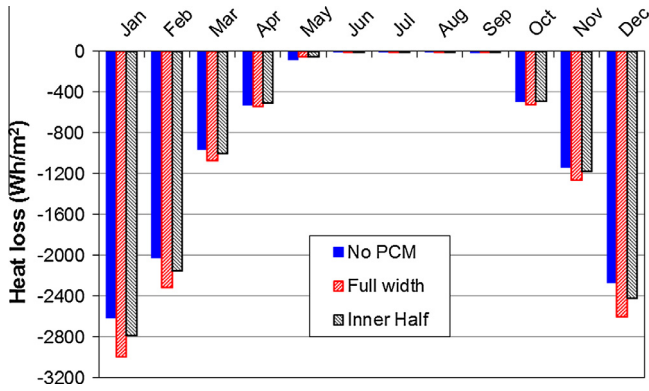


Fig. 16. Calculated monthly heat losses through the north wall, with different PCM configurations.

configuration with PCM–cellulose in the exterior half of the wall was also modeled, but that configuration fared poorly compared to the other scenarios, with both higher heat gains and losses, and has not been shown here.

For further evaluating the impact of the PCM, total integrated monthly heat gains and losses were calculated for the south and north walls, and are shown in Figs. 15 and 16. It is interesting to note the variation in the impact of the PCM on the wall heat transfer based on configuration and month (i.e. weather conditions). Highest reductions in the calculated wall heat gains with PCM were observed during the winter, spring and fall (autumn) months. In fact, during summer, the configuration with PCM in the full width of the wall allowed the highest heat gains. The calculated monthly heat losses were consistently highest for the ‘Full width’ configuration, followed by ‘Inner half’ and ‘No PCM’ configurations; the heat losses were negligible during the summer months.

4.3.3. Calculated annual electricity consumption

The previous two sub-sections described in detail, the impact of the PCM on the wall heat transfer. However, to estimate the actual

energy-saving potential of the PCM, the wall heat gains and losses need to be converted to energy consumption (electricity, natural gas, etc.). For this purpose, a typical residential heat pump was considered, with temperature-dependent coefficients of performance (COP) as shown in Fig. 17. The heat pump was assumed to be capable of operating in both cooling and heating modes. The temperature-dependent COP were calculated based on published data [31,32] for a 3-ton heat pump unit with a seasonal energy efficiency ratio (SEER) rating of 13. Both the SEER rating and tonnage chosen are typical values for heat pumps currently used in residential buildings. The COP (Wh/Wh) can be used to convert the calculated heat gains and losses into electricity consumption. It was assumed that the heat pump, while in cooling mode, operated only when the room temperature tended to exceed the cooling set point. In other words, if the room temperature remained below the cooling set point, there was no electricity consumption even if there was some heat gain through the walls. The converse was true for heating mode operation of the heat pump, i.e. the heat pump operated only when the room temperature tended to fall below the heating set point.

Childs and Stovall [30] found that, for cooling, the time-delay in peak heat gains due to PCM in walls had an added benefit of reduction in electricity use as the cooling equipment efficiency is related to the ambient temperature. The cooling equipment is very often placed in unconditioned space, and operates more efficiently, i.e. provides the same cooling performance while consuming lower electricity, when the outside temperatures are lower.

The total annual cooling and heating electricity consumption were estimated using the calculated wall heat gains and losses for all four wall orientations and the different PCM configurations, and are shown in Fig. 18. Based on the simulations, addition of PCM can reduce the total annual cooling electricity for all wall orientations. The cooling energy savings were similar whether PCM was added to the inner half of the wall cavity or the full width. This has an important implication, which is that similar cooling energy savings can be achieved at half the cost of PCM by adding PCM to only the inner half of the wall. There may be some incremental cost

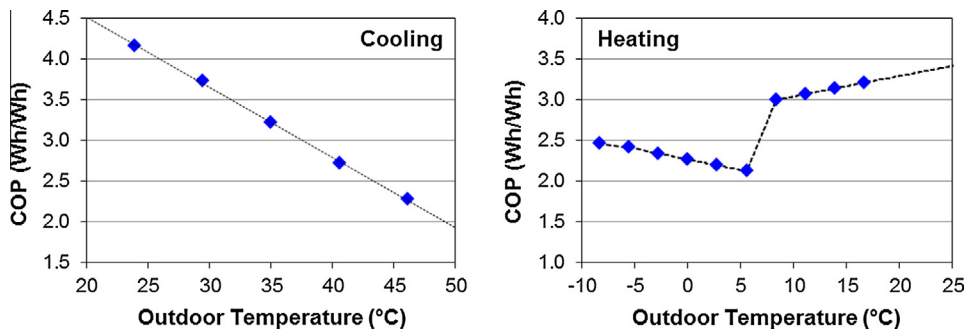


Fig. 17. Temperature-dependent coefficient of performance (COP) of a typical residential heat pump: left – cooling mode, right – heating mode.

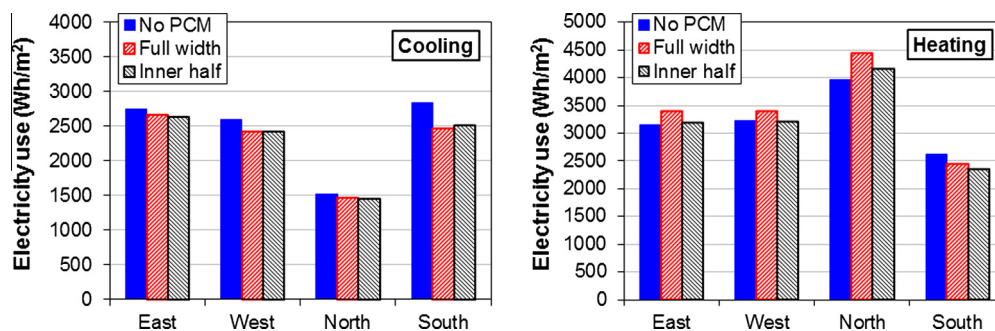


Fig. 18. Calculated annual cooling (left) and heating (right) electricity use with different PCM configurations.

Table 4
Annual heat gains and cooling electricity use with PCM–cellulose in the inner half of the wall cavity.

Wall orientation	Heat gain (Wh/m ²)		% Difference	Cooling electricity (Wh/m ²)		% Difference
	No PCM	PCM in 'Inner half'		No PCM	PCM in 'Inner half'	
East	10,451	10,150	−2.9	2,754	2,641	−4.1
West	10,143	9,641	−4.9	2,601	2,420	−7.0
North	5,761	5,665	−1.7	1,525	1,457	−4.4
South	11,289	10,193	−9.7	2,836	2,518	−11.2

Table 5
Annual heat losses and heating electricity use with PCM–cellulose in the inner half of the wall cavity.

Wall orientation	Heat loss (Wh/m ²)		% Difference	Heating electricity (Wh/m ²)		% Difference
	No PCM	PCM in 'Inner half'		No PCM	PCM in 'Inner half'	
East	−7,820	−7,812	−0.1	3,159	3,183	0.7
West	−8,139	−8,037	−1.3	3,227	3,194	−1.0
North	−10,110	−10,577	4.6	3,966	4,148	4.6
South	−6,524	−5,794	−11.2	2,625	2,348	−10.5

of the adding a partition, which needs to be considered with the cost-savings from reduced PCM quantity. Regarding heating electricity use, the 'Full width' PCM configuration actually performed worse than both the 'No PCM' and PCM in 'Inner half' configurations. Thus, from a combined cooling and heating energy consumption and cost perspectives, the PCM in 'Inner half' configuration seems optimum.

The calculated total annual heat gains and losses and electricity consumption for the 'No PCM' and PCM in 'Inner half' configurations are listed in Tables 4 and 5. Both heat gains and losses as well as cooling and heating electricity consumption were predominantly lower for the PCM in 'Inner half' configuration. It should be noted that the percent reductions in annual cooling electricity consumption with the PCM in 'Inner half' configuration were greater than the percent reduction in the heat gains, for all wall orientations.

In summary, the annual simulations showed that the low-cost bio-PCM can potentially reduce the wall-generated cooling and heating electricity consumption. Due to the variation in percent reductions in heat flows for the different wall orientations, some orientations may be more suited to PCM applications in terms of cost-effectiveness, given the local climate conditions. In the case of Charleston, the south and west walls are good candidates for application of the current PCM. Finally, as shown by Biswas et al. [25] and Childs and Stovall [30], the energy savings can be further optimized through proper choice of the phase change temperature range of the PCM with respect to the interior heating and cooling set points.

5. Conclusions and future work

In this article, experimental testing and numerical analyses of the thermal performance of a low-cost bio-PCM in an exterior wall in a hot and humid location are described. The experimental data were used to validate finite element models of the test wall containing PCM–cellulose insulation. Next, the numerical models were used to evaluate the annual impact of the PCM–cellulose insulation on the wall-generated heating and cooling loads. Annual simulations were performed using TMY3 weather data. Models of wood framed walls with both PCM–cellulose and cellulose-only insulation were created.

Different locations and distribution of the PCM were modeled to evaluate their impact on the performance of the PCM. The annual simulations showed that the PCM–cellulose insulation can reduce electricity consumption for space-conditioning, compared to cellulose-only insulation. An interesting finding was that incorporating

PCM in the inner portion of the wall cavity yielded similar cooling electricity savings as adding PCM to the entire cavity. The configuration with PCM in the inner section also improved the wall thermal performance related to heating electricity consumption, but PCM in the full cavity had an adverse impact compared to the case with no PCM. Thus, overall, adding PCM to only the inner section of an exterior wall can yield better thermal performance at lower cost than adding PCM to the entire wall cavity. The potential for energy-savings by the application of the current PCM was also dependent on the wall orientation and, based on local weather conditions, some wall orientations may be better candidates than others for PCM applications.

Further work is needed to determine an optimum set of conditions to maximize the energy savings resulting from the PCM–cellulose insulation. Two factors that could be considered are removal of the latent heat of freezing so it is not released to the building interior during summer, and phase change temperature of the PCM with respect to interior temperatures. Testing and simulations need to be performed to evaluate the performance of the PCM–cellulose insulation in other climate types. Further, the current annual simulations only considered a clear wall section, with no construction details like corners, joints with ceiling and other walls, and interactions with other walls. Also, internal loads, solar gain and heat flow through windows, roof and ceiling loads, infiltration, etc. were not considered. To get a more realistic estimate of energy savings from the PCM–cellulose insulation, whole-house modeling that considers all the above factors is required.

Acknowledgements

The authors gratefully acknowledge the funding support for this work from the United States Department of Energy as part of the American Recovery and Reinvestment Act, as Contract No. DE-EE0003924. The authors are also thankful to Jerald Atchley and Phillip Childs of ORNL for their contributions in installing and instrumenting the test wall, data gathering and troubleshooting, Drs. Keith Rice and Bo Shen (ORNL) for the heat pump coefficient of performance-related calculations, and Dr. Som Shrestha for providing the weather data used for the annual simulations.

References

- [1] Chaabane M, Mhiri H, Bournot P. Thermal performance of an integrated collector storage solar water heater (ICSSWH) with phase change materials (PCM). *Energy Convers Manage* 2014;78:897–903.

- [2] Wu W-F, Liu N, Cheng W-L, Liu Y. Study on the effect of shape-stabilized phase change materials on spacecraft thermal control in extreme thermal environment. *Energy Convers Manage* 2013;69:174–80.
- [3] Lu W, Tassou SA. Experimental study of the thermal characteristics of phase change slurries for active cooling. *Appl Energy* 2012;91:366–74.
- [4] Huang MJ, Eames PC, Norton B. Phase change materials for limiting temperature rise in building integrated photovoltaics. *Sol Energy* 2006;80:1121–30.
- [5] Zhou D, Zhao CY, Tian Y. Review on thermal energy storage with phase change materials (PCMs) in building applications. *Appl Energy* 2012;92:593–605.
- [6] Zhou G, Zhang Y, Wang X, Lin K, Xiao W. An assessment of mixed type PCM-gypsum and shape-stabilized PCM plates in a building for passive solar heating. *Sol Energy* 2007;81:1351–60.
- [7] Darkwa J, Su O. Thermal simulation of composite high conductivity laminated microencapsulated phase change material (MEPCM) board. *Appl Energy* 2012;95:246–52.
- [8] Hawes DW, Feldman D. Absorption of phase change materials in concrete. *Sol Energy Mater Sol Cells* 1992;27:91–101.
- [9] Cabeza LF, Castellon C, Nogues M, Medrano M, Leppers R, Zubillaga O. Use of microencapsulated PCM in concrete walls for energy savings. *Energy Build* 2007;39:113–9.
- [10] Shrestha S, Miller W, Stovall T, Desjarlais A, Childs K, Porter W, et al. Modeling PCM-enhanced insulation system and benchmarking EnergyPlus against controlled field data. In: *Proc building simulation 2011: 12th conf international building performance simulation association*, http://www.ibpsa.org/proceedings/BS2011/P_1328.pdf; 2011. p. 800–7.
- [11] Kosny J, Kossecka E, Brzezinski A, Tleoubaev A, Yarbrough D. Dynamic thermal performance analysis of fiber insulations containing bio-based phase change materials (PCMs). *Energy Build* 2012;52:122–31.
- [12] Aydin AA, Okutan H. Polyurethane rigid foam composites incorporated with fatty acid ester-based phase change material. *Energy Convers Manage* 2013;68:74–81.
- [13] Kosny J, Biswas K, Miller W, Kriner S. Field thermal performance of naturally ventilated solar roof with PCM heat sink. *Sol Energy* 2012;86:2504–14.
- [14] Biswas K, Kriner S, Miller W, Manlove G. A study of the energy-saving potential of metal roofs incorporating dynamic insulation systems. Thermal performance of exterior envelopes of whole buildings XII, <http://www.techstreet.com/ashrae/products/1868132#jumps>; 2013.
- [15] Meng E, Yu H, Zhan G, He Y. Experimental and numerical study of the thermal performance of a new type of phase change material room. *Energy Convers Manage* 2013;74:386–94.
- [16] Shi X, Memon SA, Tang W, Cui H, Xing F. Experimental assessment of position of macro encapsulated phase change material in concrete walls on indoor temperatures and humidity levels. *Energy Build* 2014;71:80–7.
- [17] Ascione F, Bianco N, De Masi RF, de'Rossi F, Vanoli GP. Energy refurbishment of existing buildings through the use of phase change materials: energy savings and indoor comfort in the cooling season. *Appl Energy* 2014;113:990–1007.
- [18] Zwanzig SD, Lian Y, Brehob EG. Numerical simulation of phase change material composite wallboard in a multi-layered building envelope. *Energy Convers Manage* 2013;69:27–40.
- [19] Simacek P, Kubicka D, Kubikova I, Homola F, Pospisil M, Chudoba J. Premium quality renewable diesel fuel by hydroprocessing of sunflower oil. *Fuel* 2011;90:2473–9.
- [20] Bezerigianni S, Kalogianni A, Dimitriadis A. Catalyst evaluation for waste cooking oil hydroprocessing. *Fuel* 2012;93:638–41.
- [21] Zalba B, Marin JM, Cabeza LF, Mehling H. Review on thermal energy storage with phase change: materials, heat transfer analysis and applications. *Appl Therm Eng* 2009;23:251–83.
- [22] Kosny J, Shukla N, Fallahi A. Cost analysis of simple phase change material-enhanced building envelopes in southern U.S. climates, report for U.S. Department of Energy, Fraunhofer CSE, http://cse.fraunhofer.org/Portals/55819/docs/ba_pcm_enhanced_building_envelopes.pdf; 2013.
- [23] Shukla N, Cao P, Kosny J. Lab-scale dynamic thermal testing of PCM-enhanced building materials. In: *ASTM selected technical paper (STP) – C16 symposium on next-generation thermal insulation challenges and opportunities*, Jacksonville, FL; October 23–24, 2013.
- [24] Al-Saadi SN, Zhai Z. Modeling phase change materials embedded in building enclosure: a review. *Renew Sustain Energy Rev* 2013;21:659–73.
- [25] Biswas K, Lu J, Soroushian P, Shrestha S. Combined experimental and numerical evaluation of a prototype nano-PCM enhanced wallboard. *Appl Energy* 2014;131:517–29.
- [26] Castellon C, Gunther E, Mehling H, Hiebler S, Cabeza LF. Determination of the enthalpy of PCM as a function of temperature using a heat-flux DSC: a study of the different measurement procedures and their accuracy. *Int J Energy Res* 2008;32:1258–65.
- [27] ASTM C1784-13. Standard test method for using a heat flow meter apparatus for measuring thermal storage properties of phase change materials and products. West Conshohocken, PA, USA: ASTM International; 2013.
- [28] ASTM C518-10. Standard test method for steady-state thermal properties by means of the heat flow meter apparatus. West Conshohocken, PA, USA: ASTM International; 2010.
- [29] Walton GN. Thermal analysis research program manual, NBSSIR 83-2655, National Bureau of Standards; 1983.
- [30] Childs K, Stovall T. Use of phase change material in a building wall assembly: a case study of technical potential in two climates. International high performance buildings conference at Purdue, West Lafayette, IN; July 16–19, 2012. http://www.conftool.com/2012Purdue/index.php?page=browseSessions&form_session=67.
- [31] Lennox Industries Inc. Lennox engineering data, heat pump outdoor units, XP13, Elite Series, R-410A, Bulletin No. 210432, June 2006. .
- [32] Lennox Industries Inc. Lennox engineering data, heat pump outdoor units, XP13, Elite Series, expanded rating tables, Bulletin No. 210432R, August 2007.